

1 Composition, size and cloud condensation nuclei activity of biomass burning aerosol
2 from north Australian savannah fires.

3 **Authors:**

4 Marc D. Mallet¹, Luke T. Cravigan¹, Anđelija Milic¹, Joel Alroe¹, Zoran D. Ristovski¹,
5 Jason Ward², Melita Keywood², Leah R. Williams³, Paul Selleck², Branka Miljevic^{1*}

6 **Affiliations:**

7 ¹School of Chemistry, Physics and Mechanical Engineering, Queensland University of Technology,
8 Queensland, Brisbane, 4001, Australia

9 ²CSIRO Oceans and Atmosphere Flagship, Aspendale, Victoria, 3195, Australia

10 ³Aerodyne Research, Inc., Billerica, Massachusetts, 01821, USA

11 **Corresponding author:**

12 Dr Branka Miljevic

13 Contact Phone: +71 7 3138 3827

14 Contact Email: b.miljevic@qut.edu.au

1 **Abstract**

2 The vast majority of Australia's fires occur in the tropical north of the continent during
3 the dry season. These fires are a significant source of aerosol and cloud condensation
4 nuclei (CCN) in the region, providing a unique opportunity to investigate the biomass
5 burning aerosol (BBA) in the absence of other sources. CCN concentrations at 0.5%
6 supersaturation and aerosol size and chemical properties were measured at the
7 Australian Tropical Atmospheric Research Station (ATARS) during June 2014. CCN
8 concentrations reached over 10^4 cm^{-3} when frequent and close fires were burning; up
9 to 45 times higher than periods with no fires. Both the size distribution and composition
10 of BBA appeared to significantly influence CCN concentrations. A distinct diurnal
11 trend in the proportion of BBA activating to cloud droplets was observed, with an
12 activation ratio of $40\% \pm 20\%$ during the night and $60\% \pm 20\%$ during the day. BBA
13 was, on average, less hygroscopic during the night ($\kappa = 0.04 \pm 0.03$) than during the
14 day ($\kappa = 0.07 \pm 0.05$), with a maximum typically observed just before midday. Size-
15 resolved composition of BBA showed that organics comprised a constant 90% of the
16 aerosol volume for aerodynamic diameters between 100 nm and 200 nm. While this
17 suggests that the photochemical oxidation of organics led to an increase in the
18 hygroscopic growth and an increase in daytime activation ratios, it does not explain the
19 decrease in hygroscopicity after midday. Modelled CCN concentrations assuming
20 typical continental hygroscopicities produced very large overestimations of up to
21 200%. Smaller, but still significant over predictions up to $\sim 100\%$ were observed using
22 AMS and H-TDMA derived hygroscopicities as well as campaign night and day
23 averages. The largest estimations in every case occurred during the night when the
24 small variations in very weakly hygroscopic species corresponded to large variations
25 in the activation diameters. Trade winds carry the smoke generated from these fires
26 over the Timor Sea where aerosol-cloud interactions are likely to be sensitive to
27 changes in CCN concentrations, perturbing cloud albedo and lifetime. Dry season fires
28 in north Australia are therefore potentially very important in cloud processes in this
29 region.

30 **1 Introduction**

31 Biomass burning aerosol (BBA) can act as efficient cloud condensation nuclei (CCN)
32 and form cloud droplets. Fires can therefore influence cloud formation, growth,
33 reflectance, precipitation and lifetime (Kaufman et al., 1998; Warner and Twomey,

1 1967). The contribution of CCN from fires results in higher concentrations of cloud
2 droplets, which yield whiter clouds that generally survive longer than clouds with fewer
3 droplets (Platnick and Twomey, 1994). While greenhouse gases and black carbon
4 emitted from fires absorb radiation and have a warming effect, the influence of solar
5 radiation scattering by organic material and the production of CCN has a cooling effect
6 on the Earth's lower atmosphere. The net forcing of carbonaceous combustion aerosol
7 is thought to have an overall global cooling effect (Spracklen et al., 2011; Ward et al.,
8 2012). The complexity arises from variability in emission factors, BBA size,
9 composition and aging. This contributes to a large uncertainty that these fires have on
10 the radiative budget (Carslaw et al., 2010). Thus detailed measurements of the physical
11 and chemical properties of BBA from all regions in different seasons are essential in
12 determining their impact on clouds (Spracklen et al., 2011). Very few studies have
13 taken place within Australia, despite Australia contributing an estimated 15% of yearly
14 global burned land area (van der Werf et al., 2006). Australian studies have been
15 typically focused on fires in the southern continent (Lawson et al., 2015) or east coast
16 cane fires (Warner and Twomey, 1967). The extent to which dry season fires in north
17 Australia impact CCN concentrations has not been explored in detail.

18
19 Most of central north Australia is unpopulated and is characterized by savannah
20 vegetation with grasslands, shrubs and scattered Eucalypt trees. Although the most
21 devastating fires burn in the densely populated southern regions of Australia, the vast
22 majority of the continent's fires occur in the north and are responsible for more than
23 half of land area affected by fires (Russell-Smith et al., 2007). During the dry season
24 (May until November) thousands of fires burn via prescribed burning and natural or
25 accidental ignitions. The frequency and severity of these fires increases as the season
26 progresses from the early dry season to the late dry season (Andersen et al., 2005).
27 Under Aboriginal management, fires were lit in the late dry season in order to prepare
28 for the wet season. These late dry season fires may have been lit intentionally to trigger
29 the onset of rainfall following the formation of pyro-cumulus clouds, among other
30 ecological reasons (Bowman and Vigilante, 2001; Bowman et al., 2007). Under non-
31 Indigenous management, early dry season prescribed burns are commonplace in order
32 to reduce the severity of late dry season fires (Andersen et al., 2005). Outside of the
33 only major urban center in this region, Darwin, prescribed burns are the dominant

1 source of accumulation mode aerosol particles (Mallet et al., 2016). Although long
2 range mineral dust sourced from the central Australian desert was observed during
3 SAFIRED (Winton et al., 2016), the number concentrations of these particles in the
4 sub-200 nm size range was likely to be negligible. Thus these prescribed burns will
5 dictate CCN concentrations in the region.

6
7 The vegetation (fuel) type, burning conditions and atmospheric aging determines the
8 size, composition and the hygroscopicity of BBA, and in turn their ability to act as
9 CCN. BBA is typically a mixture of elemental carbon, organic carbon and can contain
10 inorganic material (Reid et al., 2005). The precise organic carbon composition of
11 primary BBA can vary greatly depending on the fuel type and these organic constituents
12 can be weakly or highly hygroscopic (Carrico et al., 2010; Mochida and Kawamura,
13 2004; Novakov and Corrigan, 1996; Petters et al., 2009). The hygroscopicity of BBA
14 can change with oxidation and with the condensation or evaporation of volatile organic
15 compounds (VOCs) through atmospheric aging (Hennigan et al., 2011). Smog chamber
16 experiments have shown that after a few hours of simulated photochemical aging, the
17 hygroscopicity of BBA converges to weakly hygroscopic for many different fuel types
18 (Engelhart et al., 2012; Giordana et al., 2013).

19
20 While laboratory based measurements are useful in understanding the physical and
21 chemical processes that determine the hygroscopicity and composition of aerosol, they
22 do not necessarily represent ambient conditions. Due to feasibility, however, direct
23 ambient measurements of the CCN activity of smoke plumes are rare (Lawson et al.,
24 2015) and more measurements are useful in assessing the validity of climate models. A
25 previous preliminary study of the CCN activity of savannah fires in the north Australian
26 early dry season reported moderately hygroscopic BBA (Fedele, 2015), speculating that
27 the aerosol is mostly made up of aged biomass burning particles with a coating of
28 secondary organic aerosol. While these measurements took place over a short period,
29 there was a discernable slight increase in the hygroscopicity of BBA during the day.
30 Diurnal patterns in hygroscopicity have been observed in boreal environments
31 (Paramonov et al., 2013) and in the southeast United States (Cerully et al., 2015),
32 attributing increases in daytime hygroscopicity to the photochemical oxidation of
33 organic aerosol.

34

1 Some studies suggest that the impact of composition, and therefore changes in BBA
2 hygroscopicity due to photochemical aging, on CCN concentrations is much lower than
3 the impact from the aerosol size distribution (Dusek et al., 2006; Petters et al., 2009;
4 Spracklen et al., 2011). Under this assumption, changes to the activation diameter
5 resulting from a change in hygroscopicity are less important than the size distribution
6 of the BBA. Other studies have shown that while this is true for moderately and strongly
7 hygroscopic particles, cloud droplet number concentrations are moderately sensitive to
8 weakly hygroscopic particles (Reutter et al., 2009; Gácita et al., 2017)

9

10 Smoke from biomass burning can be transported over intercontinental distances and
11 can reach the upper levels of the atmosphere (Andreae et al., 2001; Dirksen et al., 2009).
12 Aircraft measurements during the early and late dry season in north Australia, however,
13 suggest that smoke from fires in this region are contained within the planetary boundary
14 layer (Ristovski et al., 2010; Kondo et al., 2003). Trade winds collect and carry this
15 smoke northwest over northern Australia, the Timor Sea and the tropical warm pool.
16 Cloud albedo is more sensitive to aerosol concentrations in pristine environments
17 (Twomey, 1991). The biomass burning that occurs during the dry season is the
18 dominant source of particles in north Australia, and is therefore likely to influence
19 aerosol-cloud interactions over the tropical warm pool in the Timor Sea.

20

21 This paper presents a comprehensive data set of the particle size, chemical composition,
22 hygroscopicity and CCN properties of BBA generated from fires in the dry season in
23 this region. The impact of BBA size and hygroscopicity on CCN activation are
24 discussed in detail. These parameters will be useful in climate models to assess the
25 magnitude of climate forcing by BBA in aerosol-cloud interactions.

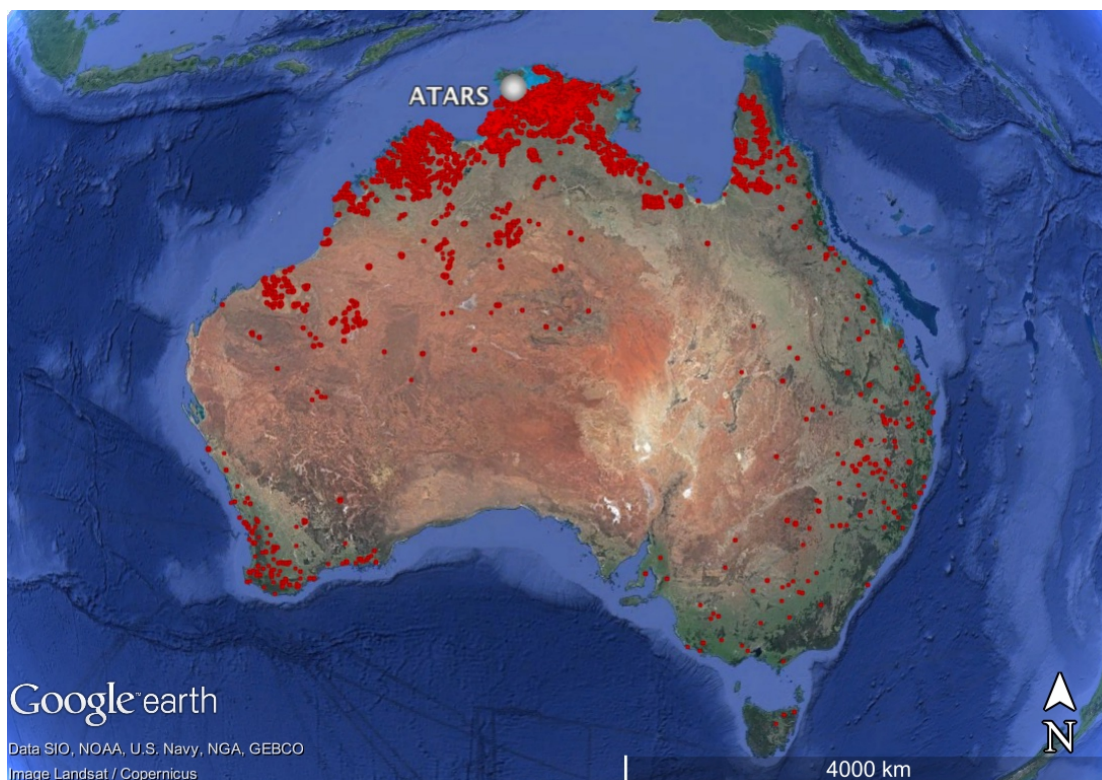
26 **2 Experimental**

27 Sampling took place at the Australian Tropical Atmospheric Research Station
28 (ATARS; 12°14'56.6"S, 131°02'40.8"E), Gunn Point, in the Northern Territory of
29 Australia as a part of the Savannah Fires in the Early Dry season (SAFIRED) campaign
30 (Mallet et al., 2016). The research station is located near the tip of a small peninsula
31 with close proximity to the Timor Sea and Tiwi Islands. The Territory capital, Darwin,
32 lies 20 km to the south west of the station. Savannah vegetation with scarce human
33 settlements transition over hundreds of kilometers to the south into the desert regions

1 of central Australia. Sampling for the SAFIRED campaign occurred in June 2014 at
2 ATARS. This period is the early dry season in this region, where strategic small-scale
3 controlled burns are performed in order to reduce the frequency and intensities of fires
4 in the late dry season in October and November. Despite sampling occurring during
5 winter, daily temperatures can reach well above 30°C such that accidental and natural
6 fires can also occur. Throughout the sampling period, thousands of fires were observed
7 in northern Australia. This led to strong biomass burning signatures detected at the
8 station, with numerous instances of very intense BBA events from both distant and
9 close fires. A full overview of the campaign, including meteorological, gaseous and
10 aerosol measurements is presented in Mallet et al. (2016).

11

12 Sentinel Hotspots, an Australian national bushfire monitoring system, was used to
13 investigate the number of daily fires in the region. Sentinel uses data from the MODIS
14 (Moderate-resolution Imaging Spectroradiometer) sensors onboard the Terra and Aqua
15 NASA satellites and the VIIRS (Visible Infrared Imaging Radiometer Suite) sensor
16 onboard the NASA/NOAA Suomi NPP satellite. These satellites fly over north
17 Australia once per day between 11:00 am and 3:00 pm local time. Although fire
18 locations are therefore limited to those that are burning during these times, Sentinel is
19 still useful in providing information on the spread and number of fires burning in the
20 region. Over the sampling period of this study, over 28000 hotspots (with a detection
21 confidence of at least 50%) were detected, with more than half of these occurring within
22 400 km of ATARS (see Figure 1). For this study, the total number of observed fires
23 within 10 km and 20 km of ATARS were also calculated (Figure 2b) for a qualitative
24 assessment of how the smoke from these fires can affect cloud condensation nuclei
25 concentrations.



1
2
3
4
5
6
7
8
9
10
11
12
13
14
15
16
17
18
19
20
21

Figure 1 The total number of detected hotspots (confidence that hotspot is fire >50%) between the 30th May 2014 and the 1st of July 2014 in Australia.

2.1 Instrumentation

Aerosol size, concentration, composition, hygroscopicity and CCN concentration measurements were taken to characterise BBA water uptake and its potential impact on cloud formation. Ambient aerosol was sampled through an automated regenerating aerosol diffusion dryer to condition the intake to below 40% relative humidity. PM₁ filters were collected on a TAPI 602 Beta plus particle measurement system (BAM) for an analysis of elemental and organic carbon. A Scanning Mobility Particle Analyzer (SMPS) made up of a TSI 3071 electrostatic classifier and TSI 3772 Condensation Particle Counter (CPC) was used to determine the particle size distributions and number concentrations between 14 nm and 650 nm with a 5 minute averaging time. A Cloud Condensation Nuclei Counter (CCNC) was used to measure total cloud droplet concentrations at a supersaturation of 0.5% every 10 seconds. A Hygroscopicity Tandem Differential Mobility Analyser (H-TDMA) alternated measurement of the hygroscopic growth factor (HGF; D/D_0) of ambient 50 and 150 nm size selected particles exposed to a relative humidity of 90% (Johnson et al., 2004).

An Aerodyne compact Time-of-Flight Aerosol Mass Spectrometer (cToF-AMS) was used to determine the size-resolved chemical composition of non-refractory sub-micron

1 aerosol. A full discussion on the cToF-AMS analysis of the composition of bulk PM₁
2 aerosol can be found in Milic et al. (2016). Briefly, in order to account for fragmentation
3 table issues during periods of high signals in which some sulphate species were
4 misattributed to organics, the high-resolution AMS analysis toolkit, PIKA, was used to
5 separate organic and sulphate signals. Data for the analysis of the size-resolved
6 chemical composition within PIKA were not recorded during the sampling period and
7 therefore the standard AMS analysis toolkit, Squirrel, was used with unit mass
8 resolution. In order to account for fragmentation table issues related to the incorrect
9 assignment of organic and sulfate species, the size-resolved mass concentrations for
10 each species were scaled by the ratio of the mass concentrations reported by the PIKA
11 analysis to the integrated mass concentrations reported by Squirrel. The size-resolved
12 composition revealed that inorganic ammonium and sulphate species made up a greater
13 contribution of larger particles than in smaller particles (Figure S1). The composition
14 of particles between 100 nm and 200 nm (aerodynamic diameter) was therefore used in
15 this study as this size range is more representative of aerosols at the CCN activation
16 diameter. This is further discussed in section 3.3.

17

18 **2.2 Analysis**

19 Total particle number concentrations (PNc) were calculated by integrating the size
20 distributions measured by the SMPS. The activation ratio of BBA as CCN at 0.5%
21 supersaturation was calculated by dividing the CCNc by the PNc. Apparent activation
22 diameters were calculated by a step-wise integration of the particle size distribution
23 from the maximum size bin towards the lower size bins until the total number of
24 particles exceeded the total number of CCN, as per:

$$CCNc = \int_{Activation\ diameter}^{Upper\ diameter} dN/d\log D_p \cdot dD_p \quad \text{Equation 1}$$

25 where CCNc is the total cloud condensation nuclei concentration, N is the particle
26 number concentration for each size bin, D_p is the particle diameter, the upper diameter
27 is the largest size measured by the SMPS (650 nm) and the activation diameter is the
28 size at which the particles activate to cloud droplets. To calculate the precise activation
29 diameter, a linear fit ($R^2 > 0.98$) between the cumulative particle number concentrations
30 and the diameter was applied across 11 size bins centered on the bin in which the
31 activation diameter falls. The uncertainty in the activation diameters was calculated
32 assuming a maximum uncertainty in the CCN concentrations of $\pm 10\%$ and was

1 typically of the order of 7 nm. The extremely vast majority of particles were observed
2 around 100 nm and, on average, only 0.07% of the number of particles measured by
3 the SMPS were between 600 and 650nm. The influence of particles larger than 650nm
4 that were not measured by the SMPS were therefore negligible on the calculation of
5 CCNC.

6
7 The apparent activation diameters were then used to calculate the average effective
8 hygroscopicity parameter, κ , for each SMPS scan following κ -Köhler theory (Petters
9 and Kreidenweis, 2007; Petters et al., 2009). According to this theory, the
10 supersaturation required to achieve a particular droplet diameter for any given particle
11 can be determined using:

$$S(D) = \frac{D^3 - D_d^3}{D^3 - D_d^3(1 - \kappa)} \exp\left(\frac{4\sigma_{s/a}M_w}{RT\rho_w D}\right) \quad \text{Equation 2}$$

12 where S is the supersaturation, D is the droplet diameter, D_d is the dry particle diameter,
13 κ is the hygroscopicity parameter, $\sigma_{s/a}$ is the surface tension of the interface between
14 the solution and air (typically 0.072 J m^{-2} as pure water is assumed), M_w is the molecular
15 weight of water, R is the universal gas constant, T is the temperature (taken as $308 \text{ K} \pm$
16 3 K in this study) and ρ_w is the density of water. For a range of D_d values, κ and D
17 values were iteratively varied until the maximum of the κ -Köhler curve was equal to
18 0.5%, the supersaturation used in the CCNC. A relationship was then found between κ
19 and D_d for the range of 45 nm up to 160 nm (Figure S2). This relationship was then
20 applied to the calculated activation diameters over the sampling period to calculate the
21 BBA κ values. The uncertainty in the activation diameter of 7 nm led to a uncertainties
22 in κ of ~ 0.05 for activation diameters between 60 nm and 80 nm, ~ 0.01 for activation
23 diameters between 80 nm 100 nm and less than 0.01 for activation diameters above 100
24 nm.

25
26 The value of κ derived from the CCNC and SMPS is the average for all particle sizes.
27 If there is not a uniform composition, this value cannot necessarily be applied to all
28 sizes of BBA. All H-TDMA data were inverted using the TDMAinv algorithm (Gysel
29 et al., 2009) and HGF distributions were kelvin-corrected for comparison between 50
30 and 150 nm particles at 90 % relative humidity. Equation 2 was then also applied to the
31 kelvin corrected HGF distributions, thereby providing distributions of κ . This also

1 provides an insight into the mixing state of the BBA, which cannot be determined from
2 the CCNC and SMPS measurements in this study.

3
4 When the surface tension of pure water is assumed, κ is regarded as the "effective
5 hygroscopicity parameter", which accounts for changes in water activity due to the
6 solute as well as any surface tension effects (Petters and Kreidenweis, 2007; Rose et
7 al., 2010; Pöschl et al., 2009). The effective hygroscopicity parameter is therefore an
8 indication of all compositional effects of an aerosol particle on water uptake. To
9 distinguish the potential effects of surface tension, values of 0.052 J m^{-2} and 0.0683 J
10 m^{-2} were also applied. Mircea et al. (2005) suggest that the surface tension at the liquid-
11 air interface of a particle depends on the concentration of carbon. The value 0.052 J m^{-2}
12 2 represents a lower limit while a surface tension of 0.0683 J m^{-2} has been observed for
13 prescribed biomass burning particulate matter in wooded areas in the USA (Asa-Awuku
14 et al., 2008). The impact of surface tension is discussed further in Section 3.5.

15
16 The overall hygroscopicity of any given particle can be determined by the volume
17 fraction and hygroscopicity of each constituent under the Zdanovskii, Stokes and
18 Robinson assumption (Chen et al., 1973; Stokes and Robinson, 1966):

$$\kappa = \sum_i \varepsilon_i \kappa_i \quad \text{Equation 3}$$

19 where κ is the overall hygroscopicity and ε_i and κ_i are the volume fractions and
20 hygroscopicities of each constituent, respectively. A modelled κ was constructed to
21 determine the influence of diurnal changes in organic and inorganic volume fractions,
22 where $\kappa_{\text{total}} = \varepsilon_{\text{org}} \kappa_{\text{org}} + \varepsilon_{\text{EC}} \kappa_{\text{EC}} + \varepsilon_{\text{inorganic}} \kappa_{\text{inorganic}}$, following the ZSR assumption. The 12-
23 hour PM_{10} BAM filters sampled from 07:00 until 19:00 and from 19:00 until 07:00 each
24 day showed no difference in the ratio of EC to (OC + EC), and therefore a constant
25 mass fraction (EC/(EC + OC)) of 10% was applied. ε_{org} , ε_{EC} and $\varepsilon_{\text{inorganic}}$ were calculated
26 using the size-resolved mass concentrations reported by the cToF-AMS and assumed
27 densities of 1.4 g cm^{-3} (Levin et al., 2014), 1.8 g cm^{-3} (Bond and Bergstrom, 2006) and
28 1.8 g cm^{-3} (Levin et al., 2014), respectively. $\kappa_{\text{inorganic}}$ and κ_{EC} were taken as 0.60
29 (Bougiatioti et al., 2016) and 0 (Petters and Kreidenweis, 2007), respectively. The
30 contribution of inorganics in this study were taken from the reported masses of sulphate,
31 nitrate and ammonium species. During the period considered for this model, other
32 inorganic species such as potassium, a marker for biomass burning, only made up a

1 small and constant contribution to the total mass and were therefore not considered. A
2 night (18:00 until 07:00) and day value of κ_{org} were varied in the applied model in order
3 to investigate any potential changes in organic hygroscopicity due to photochemistry.

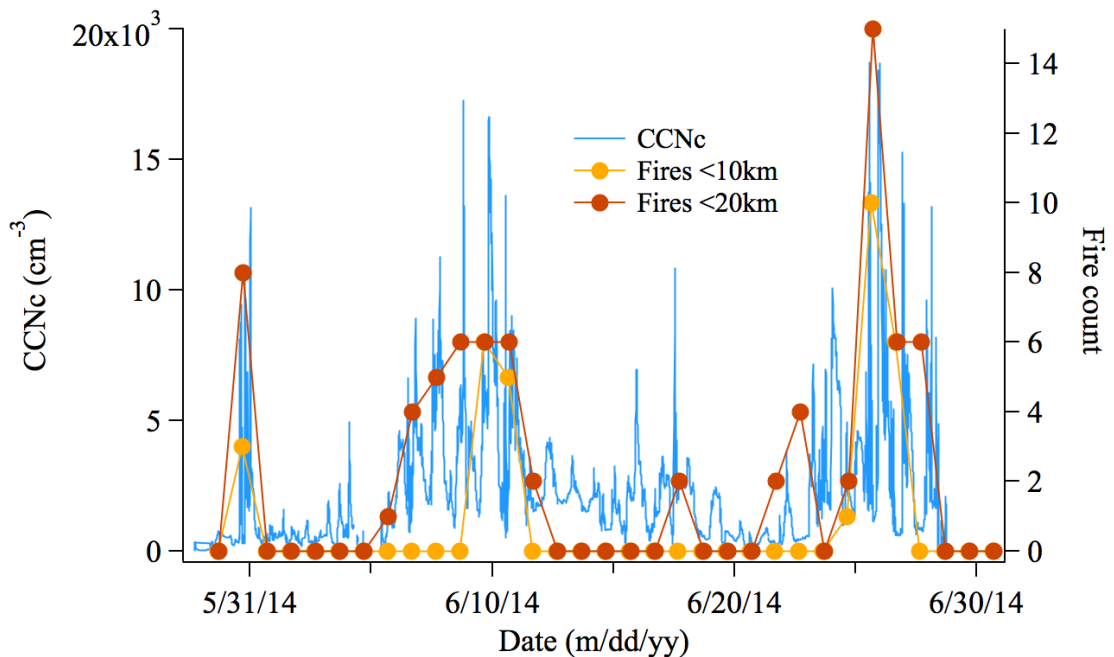
4
5 CCN concentrations were calculated in order to test prediction of CCN concentrations
6 using aerosol composition and size distribution in this region. Activation diameters
7 were derived from various hygroscopicity parameters and, again using Equation 1, the
8 size distribution was integrated step-wise from the upper size limited measured in the
9 SMPS until the activation diameter was reached. The same process used to calculate
10 the precise activation diameters earlier was used to calculate the precise CCN
11 concentrations. This process was carried out for the modelled hygroscopicity from the
12 size-resolved cToF-AMS data, the measured hygroscopicity distribution from the H-
13 TDMA as well as various constant hygroscopicity values. The constant values selected
14 were 0.05, 0.1, 0.2, 0.3 and a day and night value of 0.071 and 0.035, respectively. 0.05
15 represents the campaign average effective hygroscopicity. The day and night values
16 represent the campaign average values obtained from the SMPS-CCNC measurements.
17 The values of 0.1 and 0.2 represent commonly observed hygroscopicities for BBA in
18 other regions and in laboratory measurements Engelhart et al. (2012). The global mean
19 values of κ have been estimated to be 0.27 ± 0.21 for continental aerosols (Pringle et
20 al., 2010). It has been suggested that it is suitable to assume this continental average (κ
21 ~ 0.3) to make first order predictions of CCN activity (Rose et al., 2011). Modelling
22 CCN concentrations using these methods and assumed hygroscopicity values will
23 verify whether such values are suitable in predicting CCN activity in regions like
24 northern Australia.

25
26 In order to investigate the CCN activity of BBA, four days of unpolluted and coastal
27 conditions (19/06/2014 - 22/06/2014) were removed from the majority of the analysis.
28 Furthermore, the SMPS was only operational from 04/06/2014. Analysis of CCNc,
29 PNc, activation ratios, median particle diameters, apparent activation diameters and the
30 average effective hygroscopicity parameters are therefore only presented for data
31 collected after this date.

1 **3 Results and Discussion**

2 **3.1 BBA contribution to CCN**

3 Figure 2 shows the CCN concentrations (SS 0.5%) measured at the ATARS over the
4 campaign sampling period in June 2014 as well as the frequency of fires that were
5 observed via satellite hotspots each day within 10 km and 20 km of the station. Air
6 mass back trajectories were typically from the southeast, as were the location of the
7 fires (Mallet et al., 2016). These back trajectories revealed that the air masses did not
8 pass over Darwin or any close industrial sites, ruling out the likelihood of an urban
9 influence on CCN concentrations. The period between the 19th and 23rd of June was
10 characterized by relatively low CCN concentrations due to air originating from the
11 coastal waters of eastern Australia, which passed over minimal continental area before
12 arriving at the ATARS. As already mentioned, these dates were subsequently excluded
13 from the data analysis as the focus of this study was on the impact of BBA on CCN.
14 The highest PNC and CCN concentrations were associated with large BB events. PNC
15 concentrations of up to 400000 cm^{-3} and CCN concentrations of up to 19000 CCN cm^{-3}
16 cm^{-3} were observed during these periods.



17 *Figure 2 The time series of total cloud condensation nuclei concentrations (CCNc) at 0.5% supersaturation and the*
18 *total number of fires satellite-observed fires within 10 km (yellow) and 20 km (red) of the sampling location.*

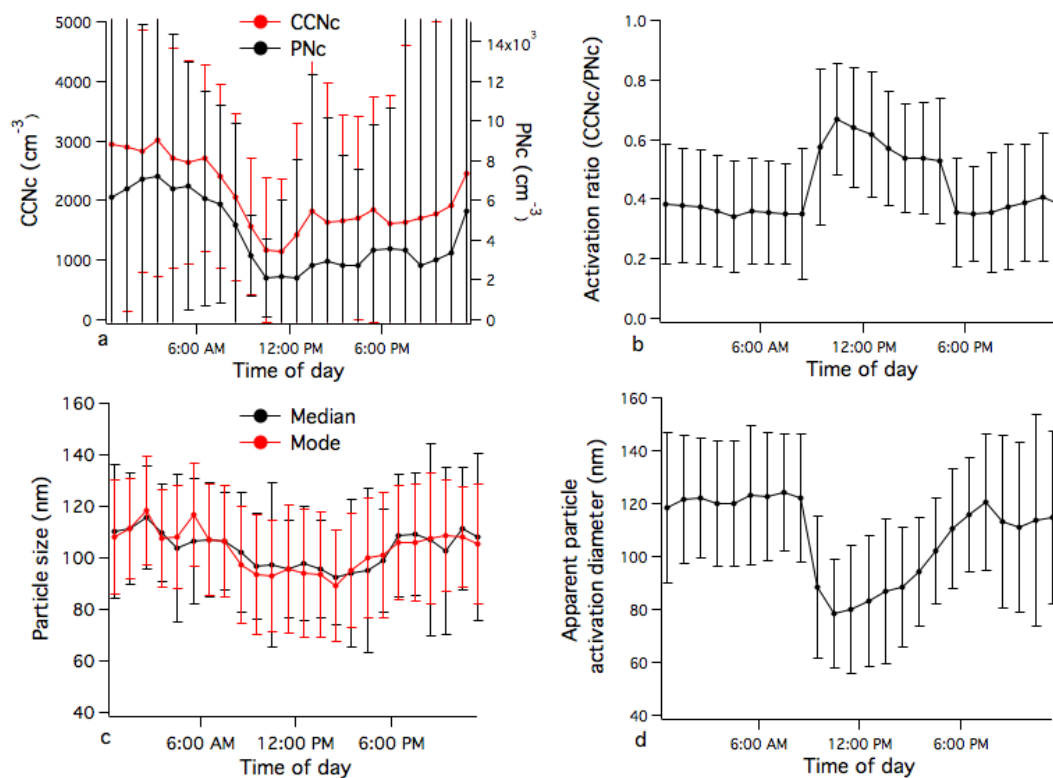
19 Although the PNC and CCN concentrations were highest during BBA events, these
20 periods were characterized by the lowest hygroscopicity and activation ratios (ratio of
21 CCNc to PNC as low as 4%). This is further discussed in Section 3.3. Activation ratios
22 typically varied between 30% and 80%, corresponding to CCN concentrations between

1 1500 cm⁻³ and 6000 cm⁻³. This contrasts observed activation ratios of over 80% in BBA
2 from dry season savannah fires in tropical southern Africa during the SAFARI 2000
3 campaign (Ross et al., 2003), despite lower supersaturations of ~0.3%. The size
4 distributions of BBA observed during SAFIRED had a count median diameter of 107
5 nm ± 25 nm, while the median diameters were typically above 150 nm in the SAFARI
6 2000 campaign, which could explain the lower activation ratios observed here. The size
7 distributions observed in this study were typically smaller than those observed in aged
8 and regional BBA on other continents (Reid et al., 2005). When particles are smaller,
9 the critical diameter for cloud droplet formation becomes more important. It is therefore
10 crucial to investigate the impact of composition on the activation diameter, and thus
11 CCN concentrations.

12

13 **3.2 Diurnal trends in BBA**

14 Diurnal patterns in the BBA PNC, CCNC, size and activation ratio and activation
15 diameter are shown in Figure 3. For most of the campaign, particle size distributions
16 were unimodal and therefore the median and mode of these distributions are used here
17 to represent the particle size. The highest concentrations of CCN were observed during
18 the night when they were also the most variable (Figure 3a). This is likely a result of
19 prescribed burns occurring later in the day or evening as well as a lower inversion layer
20 during the night. Interestingly, the activation ratio also follows a distinct diurnal trend
21 with ~40% ± 20% of BBA acting as CCN at 0.5% supersaturation during the night and
22 ~60% ± 20% during the day (Figure 3b). Smaller particles were typically seen during
23 the day than during the night (Figure 3c), indicating that it was the change in the particle
24 activation diameter (Figure 3d) that was responsible for this increase in daytime
25 activation ratios. The decrease in the particle size could possibly be explained by
26 changes in combustion (Carrico et al., 2016) of vegetation across the day, with more
27 flaming, rather than smoldering, conditions expected to be favoured during daylight
28 hours. Without more information on the exact location, fuel type and combustion
29 conditions, however, it is difficult to make conclusions about this.



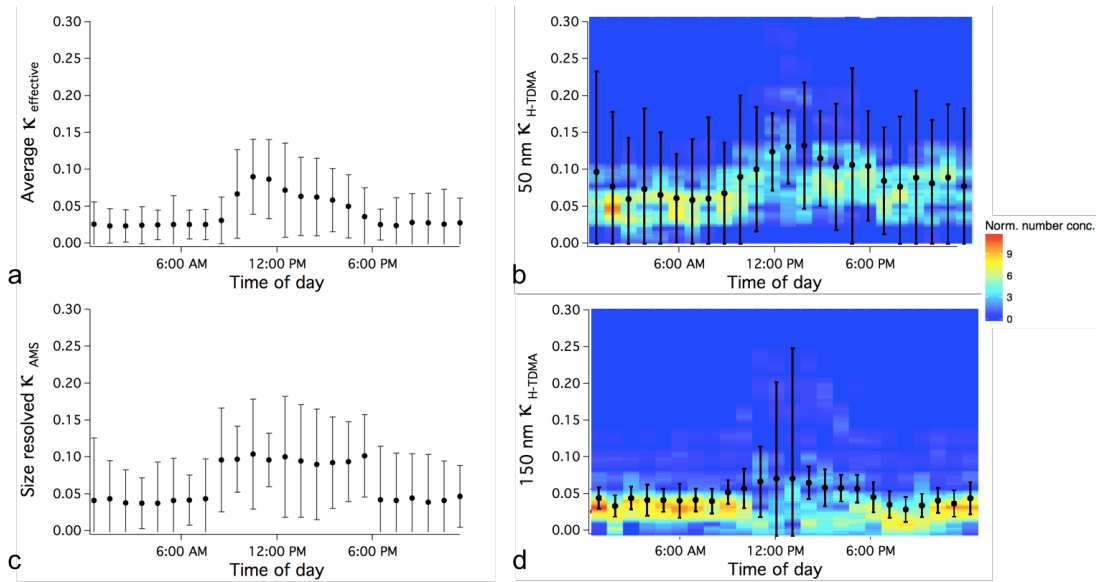
1

2 *Figure 3 The diurnal trends of a) the total cloud condensation nuclei concentration (CCNc) and particle number*
 3 *concentration (PNc), b) the activation ratio at 0.5% supersaturation, c) the median and mode of the particle size*
 4 *distribution and d) the apparent activation diameter. All reported values are the median of the hourly averaged data*
 5 *for the sampling period and the error bars represent the standard deviation.*

6 The hygroscopicity of BBA derived from the size-resolved AMS, CCNC/SMPS and
 7 the H-TDMA followed a distinct diurnal trend (Figure 4). The CCNC-derived
 8 hygroscopicity (Figure 4a) during the night time (defined as 18:00 until 07:00 local
 9 time) was generally very stable and constant over the sampling period at 0.03 ± 0.03 .
 10 Daytime hygroscopicity (07:00 until 18:00) was typically higher with much more
 11 variability at 0.07 ± 0.05 . H-TDMA-derived hygroscopicities for 150 nm diameter
 12 particles (Figure 4d) agreed very well with these values, although a much higher
 13 variability was observed around noon. The hygroscopicity distributions of 50 nm
 14 diameter particles followed a similar trend but were, interestingly, slightly higher than
 15 the 150 nm distributions. The variability in hygroscopicity for 50 nm diameter particles
 16 is much greater than for 150 nm particles, due to lower concentrations at 50 nm.
 17 Hygroscopicity distributions for both 50 nm and 150 nm aerosols during the night
 18 indicate a strong internal mixture of very weak hygroscopic BBA, and during the day
 19 an increase and broadening of the hygroscopicity mode, suggesting an external mixture
 20 of slightly more hygroscopic particles. The size-resolved AMS hygroscopicity values
 21 were calculated assuming κ_{org} of 0.02 and 0.08 during the night and day, respectively.

1 The organic volume fraction was invariable (see section 3.3), therefore the increase and
 2 decrease at sunrise and sunset, respectively, is driven by the choice of night and day
 3 organic hygroscopicity values. These values were selected as they gave the best
 4 agreement between the modelled and measured CCN concentrations, which is
 5 discussed further in Section 3.4.

6
 7 Literature on the diurnal variability of BBA hygroscopicity is rare. Diurnal and
 8 afternoon averages of κ for BBA in the Amazonian dry season have been reported as
 9 0.048 and 0.072, respectively (Gácita et al., 2017), consistent with the results presented
 10 here. A short study (Fedele, 2015) carried out in 2010 at the ATARS also reported κ
 11 values in the early dry season over a period of two weeks. They showed κ values mostly
 12 between 0.05 and 0.1 for supersaturations of 0.38%, 0.68% and 0.96%, with the higher
 13 values generally occurring during the day. They directly measured the critical diameter
 14 and used an approximation presented in Petters and Kreidenweis (2007) to calculate κ .
 15 This approximation is more appropriate for κ values over 0.2, which means that the
 16 reported values between 0.05 and 0.1 were slightly overestimated and would likely be
 17 more in line with the BBA hygroscopicity observed in this study. Although a detailed
 18 chemical analysis was not done during that study, these similar values of κ suggest that
 19 these observations could be representative of early dry season fires in this region.

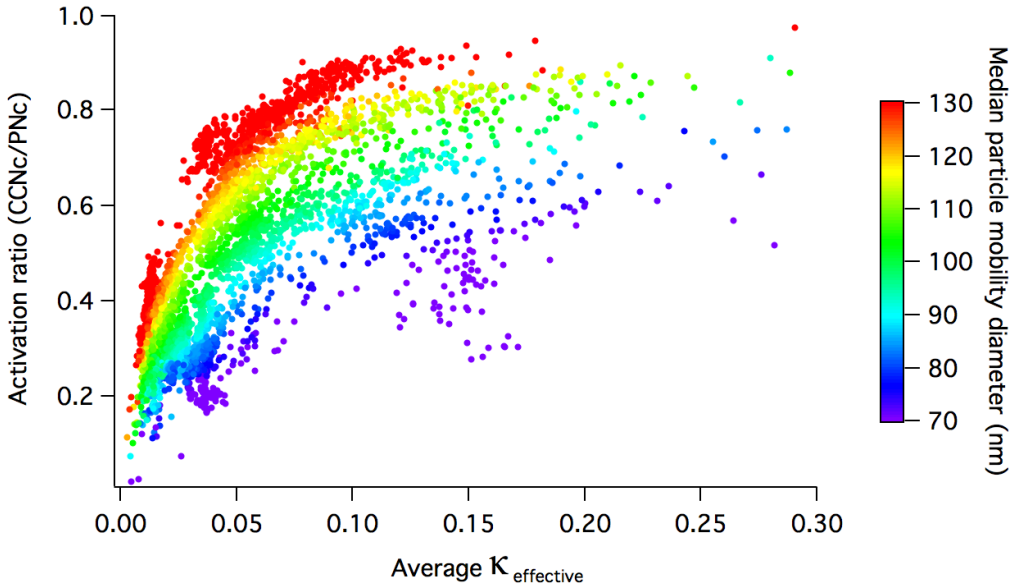


20

21 *Figure 4 The diurnal trends of a) the CCNC-derived effective hygroscopicity parameter, b) the H-TDMA derived*
 22 *kelvin-corrected hygroscopicity distributions of 50 nm particles, c) the AMS-derived hygroscopicity parameter for*
 23 *aerodynamic diameters between 100 nm and 200 nm, assuming κ_{org} of 0.02 and 0.08 during the night and day,*
 24 *respectively and d) the H-TDMA derived kelvin corrected hygroscopicity distributions of 150 nm particles. The*
 25 *black dots on b) and d) represent the hourly median hygroscopicity values and the error bars represent the standard*
 26 *deviation*

1 **3.3 BBA composition**

2 The activation ratio as a function of the effective hygroscopicity parameter, κ , as
3 calculated from equations 1 and 2, with colors indicating the median particle mobility
4 diameter, is displayed in Figure 4. This figure clearly demonstrates that both the size
5 and composition of the BBA can have a significant effect on CCN activation. For
6 example, with a constant particle size increases the CCN activation ratio from below
7 20% to above 80%. For a constant κ of 0.05 and an increase in the particle median
8 diameter from 60 nm up to 140 nm, the CCN activation ratio increases by
9 approximately 50%. The effect of composition appears to have less of an influence at
10 higher hygroscopicities, with the size being the determining factor in CCN activation
11 above a κ of 0.1. For very weakly hygroscopic ($\kappa < 0.05$) BBA, the sensitivity of particle
12 size was less prominent, with an activation ratio increase of $\sim 0.3\% \text{ nm}^{-1}$, compared to
13 a $\sim 0.7\% \text{ nm}^{-1}$ increase when $\kappa > 0.05$. These findings support the idea that cloud droplet
14 number concentrations are sensitive to composition at low hygroscopicities (Reutter et
15 al., 2009). Neglecting the effect of BBA composition in this case would lead to
16 difficulties in appropriately quantifying CCN activation.



17
18 *Figure 5 The activation ratio (CCNc/PNc) as a function of the effective hygroscopicity parameter, κ . The colours*
19 *represent the median particle mobility diameter.*

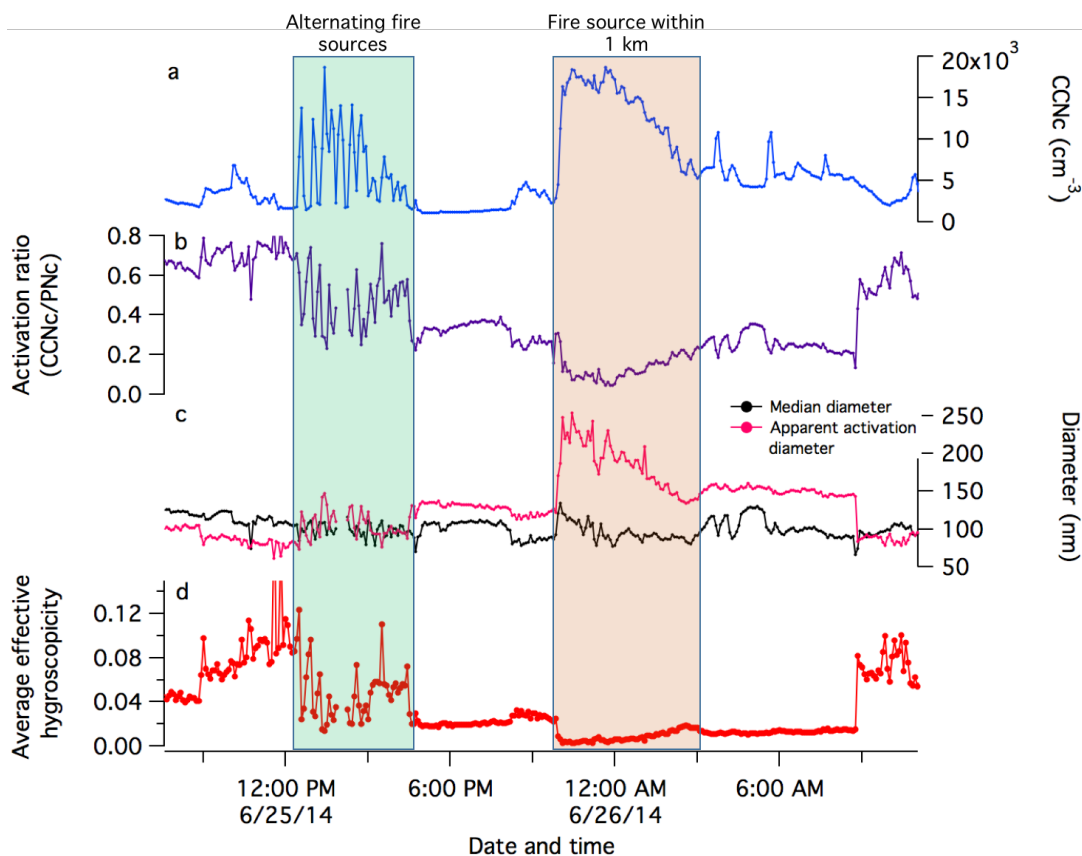
20 In order to understand the underlying causes of the variations in the hygroscopicity, the
21 size-resolved chemical composition was investigated. For bulk PM_{10} composition, there
22 was a distinct increase in the inorganic mass fractions during the day due to an
23 enrichment of ammonium and sulphate species. The size-resolved composition,
24 however, revealed that these inorganic species were more present on larger particles

1 and had a $d_{\text{aerodynamic}}$ mode at approximately 350 nm, while organics had a mode at
2 approximately 250 nm. This observation is consistent with other studies that show that
3 smaller particles are more enriched with organics (Levin et al., 2014; Rose et al., 2011;
4 Gunthe et al., 2009). As the influence of composition on CCN activation is irrelevant
5 at larger sizes, it is important to investigate the composition at smaller sizes where the
6 aerosol number is highest and the composition can affect the activation diameter. The
7 size-resolved composition revealed that, within the aerodynamic diameter size range of
8 100 nm to 200 nm, organics were completely dominant and the organic volume
9 fraction, ϵ_{org} , was invariable at approximately 90%. At least some of the increase in the
10 observed hygroscopicity and the inferred κ_{org} is likely a result of the photochemical
11 oxidation of the organics. The aging of biomass burning aerosol is discussed in further
12 depth in Milic et al. (2016), where the fraction of m/z 44 to total organics measured by
13 the AMS, a proxy for the degree of oxidation, was shown to increase steadily
14 throughout the day. As shown in Figure 4, the derived hygroscopicity values from the
15 CCNc, SMPS and H-TDMA show a decrease in the hygroscopicity soon after the peak
16 at midday. If the photochemical oxidation of organics were the sole contributor to the
17 daytime increase in hygroscopicity then it should be expected that the hygroscopicity
18 would also increase steadily throughout the day (in the absence of a change in the mass
19 fraction of inorganics). While there was no change in wind direction until later in the
20 afternoon, the peak in hygroscopicity did correspond with the peak in wind speed (see
21 Supplementary Figure S4), although it is not apparent how or if a decrease in the wind
22 speed could lead to a decrease in the hygroscopicity. A separate explanation could be
23 related to the size-dependent composition of BBA. The size resolved composition from
24 the AMS across the range of 100-200 nm was selected due to the inefficient
25 transmission of particles below 100 nm. As shown in Figure 3d, the apparent activation
26 diameter during the day decreased to approximately 80 nm. It could be that the
27 composition between 100 and 200 nm is therefore not perfectly representative of the
28 BBA at the activation diameter. Furthermore, the influence of other inorganics not
29 considered in the model of hygroscopicity or the role of surface chemistry could be
30 underestimated, leading to poor characterisation of hygroscopicity by bulk
31 composition.

32

33 While it is likely that most of the BBA observed during the SAFIRED campaign had
34 undergone some form of aging (physical or chemical), two events provided insight into

1 the characteristics of extremely fresh BBA and are described in Mallet et al. (2016).
2 During mid-afternoon on the 25th June, grass and shrub fires were blazing ~1 km
3 southeast of the ATARS site. Wind directions during this period were very unstable
4 and frequently altering between southeasterly and northeasterly. This resulted in the
5 sampled air mass frequently changing from the "fresh" plume and more background
6 like conditions over the course of approximately 4 hours. During this time, CCN
7 concentrations varied frequently between $\sim 2000 \text{ cm}^{-3}$ and $\sim 19000 \text{ cm}^{-3}$. The activation
8 ratio, median particle size, activation diameter and hygroscopicity varied between 20%
9 and 75%, 80 nm and 110 nm, 130 nm and 80 nm and 0.02 and 0.1 respectively (see
10 Figure 6). These fires continued to blaze into the evening, slowly advancing to within
11 1 km south of the ATARS site. Due to northeasterly winds, the air mass from this fire
12 wasn't observed until approximately 10 pm that night when winds became southerly.
13 For the next four hours, CCN concentrations peaked at $\sim 19000 \text{ cm}^{-3}$, despite the
14 activation ratio dropping to 4%. The average effective hygroscopicity during this event
15 dropped to 0.003 and slowly increased over the period of the fire to ~ 0.02 . This led to
16 a decrease in the apparent activation diameter from 250 nm to 150 nm, subsequently
17 increasing the CCN activation ratio to 25%. Whether this is a result of a change in the
18 burning conditions, fuel load or a combination of both is unclear. These events
19 demonstrate the importance of BB as a source of CCN, despite the relatively
20 hydrophobic nature of BBA. Furthermore, in the absence of photochemical aging, the
21 slight variation in BBA hygroscopicity during the night fire demonstrates the variability
22 of CCN activation, even over the course of an individual fire.
23



1
2
3
4
5
6

Figure 6 The CCNc, activation ratio, median particle diameter, apparent activation diameter and average effective hygroscopicity parameter during two periods with close proximity (<1 km) fires. The green shaded area indicates the period where the wind direction was periodically changing between southeasterly and northeasterly. The red shaded area indicates the period where emissions were from a grass fire burning less than 1 km from the sampling site.

7 The hygroscopicity of fresh and aged BBA has been studied extensively in laboratory
 8 smog chambers. Some studies have shown that the photochemical oxidation of organics
 9 in BBA leads to an increase in hygroscopicity (Carrico et al., 2010; Petters et al., 2009;
 10 Engelhart et al., 2012) while others suggest that the hygroscopicity converges from
 11 highly ($\kappa = 0.6$) or weakly ($\kappa = 0.06$) hygroscopic values to a value of approximately
 12 0.2 ± 0.1 (Engelhart et al., 2012). The observation of the close proximity fire event on
 13 the evening of the 25th of June (Figure 6), as well as the diurnal trends in the calculated
 14 hygroscopicity parameter (Figure 4), indicate that the composition of BBA during the
 15 night is characteristic of very weakly hygroscopic fresh BBA. The high frequency of
 16 fires during the early dry season in north Australia likely results in the "regional haze"
 17 predominantly being composed of relatively fresh BBA with a very low hygroscopicity.
 18 The aging processes were observed to increase the hygroscopicity to $\sim 0.08 \pm 0.05$,
 19 which is the lower estimate of value suggested by Engelhart et al. (2012) and smaller
 20 than other studies investigating BBA (Bougiatioti et al., 2016). Whether the
 21 hygroscopicity would converge to higher values in the absence of frequent fires or as

1 the smoke travels away from the continent is something that needs to be explored in
2 future measurements.

3

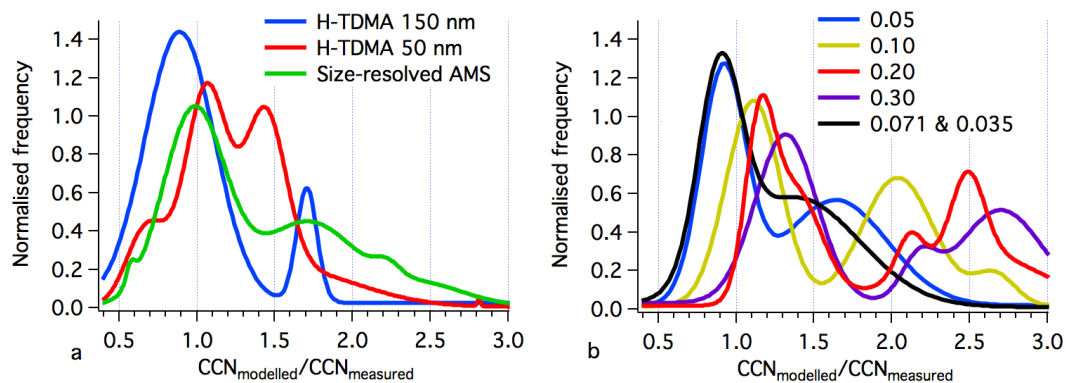
4 **3.4 Validation of modelled CCN**

5 Detailed temporal-spatial measurements of CCN concentrations are difficult and
6 therefore assumptions must be made about the size-resolved composition and water
7 uptake for similar regions and sources. Many studies have attempted closure between
8 composition, size and CCN concentrations in order to assess the validity of these
9 assumptions (Rose et al., 2010). These studies typically agree that for most
10 environments, where hygroscopicities are moderate, the size distribution and number
11 concentration of particles are the determining factor of CCN concentrations (Dusek et
12 al., 2006). Gacita et al. (2017) however, showed that for Amazonian BBA (with
13 measured $\kappa = 0.04$), applying an assumed κ of 0.20 resulted in a 26.6% to 54.3%
14 overestimation of CCN concentrations. They suggest that κ values recommended for
15 continental and BBA are too high to describe CCN behavior of Amazonian BBA. This
16 is also the case for the SAFIRED campaign.

17

18 Figure 7 shows the normalised frequency distributions of the ratio of modelled and
19 measured CCN concentrations for five different compositional scenarios, taking into
20 account the time-dependent size distributions. The smoothed curves were obtained
21 frequency distributions of these ratios, using Igor Pro's Multi-peak Fitting package. For
22 a constant hygroscopicity of 0.20, daytime concentrations were overestimated by 15%
23 to 40% while night concentrations were overestimated by well over 100%. A similar
24 case is observed for hygroscopicities of 0.10 and 0.30. For an assumed constant κ of
25 0.05, which represents the campaign average, the modelled CCN concentrations
26 slightly underestimate the measured CCN concentrations during the day by less than
27 10%, but overestimate the night CCN by 65%. Using the day and night campaign
28 averages of 0.071 and 0.035, respectively, improved the night time concentration to an
29 overestimation of approximately 50%. Using the time dependent size-resolved AMS
30 composition and assigning κ_{org} as 0.08 and 0.02 for day and night, respectively,
31 also provides a good agreement between the estimated and measured daytime CCN
32 concentrations, but again overestimates the night concentrations by 70%. H-TDMA
33 hygroscopicity distributions showed that the night was predominantly characterised by

1 an internal mixture, suggesting that the disagreement between modeled and measured
 2 CCN is due to is due to variability in fuel or burning conditions of the fires and/or night
 3 time aging. The modelled CCN concentrations from both the 50 nm and 150 nm H-
 4 TDMA were within 10% during the day, but there were also overestimations of between
 5 45% and 70% respectively. The time resolution of the H-TDMA limited the number of
 6 CCN model calculations that could be done, which introduced more potential bias for
 7 individual periods where the agreement between the measured and modelled CCN was
 8 worse (or better). The difficulty in sufficiently modelling night time CCN
 9 concentrations highlights the need for further composition measurements of fresh BBA
 10 in this region.



11
 12 *Figure 7 The normalised probability density functions for the frequency of the ratio of the modelled and measured*
 13 *CCN concentrations based on a) the 150 nm and 50 nm H-TDMA derived hygroscopicities and size-resolved cToF-*
 14 *AMS composition and b) the campaign average hygroscopicity, $\kappa=0.05$, typical BB hygroscopicities of 0.1 and 0.2,*
 15 *the continental average hygroscopicity of 0.3 and the day and night average effective hygroscopicity values of 0.071*
 16 *and 0.035, respectively.*

17 **3.5 Effect of surface tension**

18 The κ values reported in this study represent the effective hygroscopicity parameter,
 19 which accounts for all compositional effects on aerosol water uptake (i.e. solubility of
 20 components and the reduction in surface tension to their presence). This study has
 21 shown that the effective hygroscopicity parameter increases during daylight hours,
 22 speculating that this is caused by the photochemical oxidation of organics. Although
 23 surface tension measurements were not performed, using a value observed in a previous
 24 BB study of 0.0638 J m^{-2} (Asa-Awuku et al., 2008) in the κ -Köhler equation shows only
 25 a slight decrease in hygroscopicity compared to using the surface tension of pure water
 26 (Figures S2 and S3). This suggests that it is the solubility, rather than the reduction of
 27 surface tension, of the organics and inorganics present in the BBA that is responsible
 28 for the water uptake. On the other hand, an assumed lower estimate surface tension of
 29 0.052 J m^{-2} (Mircea et al., 2005) during the day could explain the increase in CCN

1 activation. Although models generally use the effective hygroscopicity parameter
2 (Pringle et al., 2010) due to the ease of using a single parameter, a better understanding
3 of the precise mechanisms that facilitate the uptake of water onto potential cloud
4 droplets is needed (Noziere, 2016).

5 **4 Conclusions**

6 Measurements at ATARS showed a strong link between the frequency of early dry
7 season fires and the concentrations of CCN, indicating that these fires are an important
8 source of CCN in northern Australia. The aerosol size distribution was typically
9 unimodal with a median diameter of 107 nm and the BBA was weakly hygroscopic and
10 predominately internally mixed. These conditions meant that both the composition and
11 size were important in determining the CCN activation of the BBA. A distinct diurnal
12 trend in the ratio of activated cloud condensation nuclei at 0.5% supersaturation and
13 particle number was observed, with $\sim 40\% \pm 20\%$ of BBA acting as CCN during the
14 night and $\sim 60\% \pm 20\%$ during the day. This increase in CCN activity corresponded
15 with an increase in the hygroscopicity from 0.04 ± 0.03 to 0.07 ± 0.05 . This was likely
16 due to the daytime photochemical oxidation of organic compounds within BBA,
17 although other factors such as changes in sub-100 nm inorganic contributions or surface
18 chemistry were likely also contributing factors. While not investigated in this study,
19 this smoke has the potential to penetrate into the upper levels of the troposphere,
20 particularly as the dry season progresses, and it also flows over the Timor Sea where
21 change in cloud albedo and lifetime is likely to be sensitive to CCN concentration
22 changes. In the case of northern Australian dry season fires, assuming typical
23 continental hygroscopicities of 0.10, 0.20 and 0.30 led to CCN overestimates of 10%
24 to 30% during the day and 100% to over 150% during the night. It is therefore important
25 that the CCN activation be better modelled.

26
27 BBA related CCN concentrations are likely to be further enhanced throughout the dry
28 season as temperatures increase and there are more frequent fires. Long term
29 monitoring or future measurements later in the dry season would allow a more detailed
30 analysis into the seasonal relationship between fire frequency, intensity and CCN.
31 Other aerosol-cloud interactions are likely to change as the season progresses. Higher
32 solar radiation and relative humidity during the late dry season lead to the formation of
33 pyro-cumulous clouds and higher rainfall in comparison to the early dry season

1 (Bowman et al., 2007). Long term measurements could also be further integrated in
2 with satellite data, such as the Burned Area Product measured by the MODIS sensors.
3 While the number of fires detected in this study is useful for a qualitative assessment
4 of the impact of fires on CCN concentrations, the area burned is likely to be a more
5 quantitative proxy for BBA emissions.

6

7 Concurrent aircraft measurements would be required to investigate the penetration and
8 evolution of smoke into upper levels of the troposphere. Characterising the presence of
9 smoke within, below and above clouds is required to fully understand the vertical
10 radiative effect of these fires. The south easterly trade winds carry this smoke over
11 waters in the Indian and western Pacific oceans known as the tropical warm pool.
12 Measurements in Indonesia or on a ship in the Timor Sea would therefore also be useful
13 in determining the long-range transport and evolution of the smoke. Furthermore, a
14 mobile sampling chamber positioned downwind of prescribed burns that occur in this
15 region, both during the day and night, would be beneficial in understanding the
16 variability of the composition of freshly emitted BBA.

17 **Data availability**

18 Data can be accessed upon request to the corresponding author (Branka Miljevic;
19 b.miljevic@qut.edu.au)

20 **Author contributions**

21 Marc Mallet wrote the manuscript, designed and conducted experimental work and
22 analysed and interpreted data. Luke Cravigan designed and conducted experimental
23 work and contributed to writing the manuscript, data analysis and data interpretation.
24 Anđelija Milic analysed data and reviewed the manuscript. Joel Alroe designed
25 experimental work, analysed data and reviewed the manuscript, Zoran Ristovski
26 designed experimental work and reviewed the manuscript. Jason Ward designed
27 experimental work and conducted experimental work. Melita Keywood led the
28 SAFIRED campaign and reviewed the manuscript. Leah Williams contributed to the
29 experimental work and reviewed the manuscript. Paul Selleck designed experimental
30 work and analysed data. Branka Miljevic designed and conducted experimental work
31 and reviewed the manuscript.

1 **References**

- 2 Andersen, A. N., Cook, G. D., Corbett, L. K., Douglas, M. M., Eager, R. W., Russell-
3 Smith, J., Setterfield, S. A., Williams, R. J., and Woinarski, J. C.: Fire frequency and
4 biodiversity conservation in Australian tropical savannas: implications from the
5 Kapalga fire experiment, *Austral Ecology*, 30, 155-167, 2005.
- 6 Andreae, M., Artaxo, P., Fischer, H., Freitas, S., Grégoire, J. M., Hansel, A., Hoor, P.,
7 Kormann, R., Krejci, R., and Lange, L.: Transport of biomass burning smoke to the
8 upper troposphere by deep convection in the equatorial region, *Geophysical Research*
9 *Letters*, 28, 951-954, 2001.
- 10 Asa-Awuku, A., Sullivan, A., Hennigan, C., Weber, R., and Nenes, A.: Investigation
11 of molar volume and surfactant characteristics of water-soluble organic compounds in
12 biomass burning aerosol, *Atmospheric Chemistry and Physics*, 8, 799-812, 2008.
- 13 Bond, T. C., and Bergstrom, R. W.: Light absorption by carbonaceous particles: An
14 investigative review, *Aerosol science and technology*, 40, 27-67, 2006.
- 15 Bougiatioti, A., Bezantakos, S., Stavroulas, I., Kalivitis, N., Kokkalis, P., Biskos, G.,
16 Mihalopoulos, N., Papayannis, A., and Nenes, A.: Biomass-burning impact on CCN
17 number, hygroscopicity and cloud formation during summertime in the eastern
18 Mediterranean, *Atmospheric Chemistry and Physics*, 16, 7389-7409, 2016.
- 19 Bowman, D., and Vigilante, T.: Conflagrations: the culture, ecology and politics of
20 landscape burning in the north Kimberley, *Ngoonjook*, 38, 2001.
- 21 Bowman, D. M., Dingle, J. K., Johnston, F. H., Parry, D., and Foley, M.: Seasonal
22 patterns in biomass smoke pollution and the mid 20th - century transition from
23 Aboriginal to European fire management in northern Australia, *Global Ecology and*
24 *Biogeography*, 16, 246-256, 2007.
- 25 Carrico, C., Petters, M., Kreidenweis, S., Sullivan, A., McMeeking, G., Levin, E.,
26 Engling, G., Malm, W., and Collett Jr, J.: Water uptake and chemical composition of
27 fresh aerosols generated in open burning of biomass, *Atmospheric Chemistry and*
28 *Physics*, 10, 5165-5178, 2010.
- 29 Carrico, C. M., Prenni, A. J., Kreidenweis, S. M., Levin, E. J., McCluskey, C. S.,
30 DeMott, P. J., McMeeking, G. R., Nakao, S., Stockwell, C., and Yokelson, R. J.:
31 Rapidly evolving ultrafine and fine mode biomass smoke physical properties:
32 Comparing laboratory and field results, *Journal of Geophysical Research:*
33 *Atmospheres*, 121, 5750-5768, 2016.
- 34 Carslaw, K., Boucher, O., Spracklen, D., Mann, G., Rae, J., Woodward, S., and
35 Kulmala, M.: A review of natural aerosol interactions and feedbacks within the Earth
36 system, *Atmospheric Chemistry and Physics*, 10, 1701-1737, 2010.
- 37 Cerully, K., Bougiatioti, A., Hite Jr, J., Guo, H., Xu, L., Ng, N., Weber, R., and Nenes,
38 A.: On the link between hygroscopicity, volatility, and oxidation state of ambient and
39 water-soluble aerosols in the southeastern United States, *Atmospheric Chemistry and*
40 *Physics*, 15, 8679-8694, 2015.
- 41 Chen, H., Sangster, J., Teng, T., and Lenzi, F.: A general method of predicting the water
42 activity of ternary aqueous solutions from binary data, *The Canadian Journal of*
43 *Chemical Engineering*, 51, 234-241, 1973.
- 44 Dirksen, R. J., Folkert Boersma, K., De Laat, J., Stammes, P., Van Der Werf, G. R.,
45 Val Martin, M., and Kelder, H. M.: An aerosol boomerang: Rapid around - the - world
46 transport of smoke from the December 2006 Australian forest fires observed from
47 space, *Journal of Geophysical Research: Atmospheres*, 114, 2009.

1 Dusek, U., Frank, G., Hildebrandt, L., Curtius, J., Schneider, J., Walter, S., Chand, D.,
2 Drewnick, F., Hings, S., and Jung, D.: Size matters more than chemistry for cloud-
3 nucleating ability of aerosol particles, *Science*, 312, 1375-1378, 2006.

4 Engelhart, G., Hennigan, C., Miracolo, M., Robinson, A., and Pandis, S. N.: Cloud
5 condensation nuclei activity of fresh primary and aged biomass burning aerosol,
6 *Atmospheric Chemistry and Physics*, 12, 7285-7293, 2012.

7 Fedele, R. M.: Observations of Australian Cloud Condensation Nuclei (CCN), RMIT
8 University, 2015.

9 Gácita, M. S., Longo, K. M., Freire, J. L., Freitas, S. R., and Martin, S. T.: Impact of
10 mixing state and hygroscopicity on CCN activity of biomass burning aerosol in
11 Amazonia, *Atmospheric Chemistry and Physics*, 17, 2373-2392, 2017.

12 Gunthe, S. S., King, S. M., Rose, D., Chen, Q., Roldin, P., Farmer, D. K., Jimenez, J.
13 L., Artaxo, P., Andreae, M. O., Martin, S. T., and Poschl, U.: Cloud condensation nuclei
14 in pristine tropical rainforest air of Amazonia: size-resolved measurements and
15 modeling of atmospheric aerosol composition and CCN activity, *Atmospheric
16 Chemistry and Physics*, 9, 7551-7575, 2009.

17 Gysel, M., McFiggans, G., and Coe, H.: Inversion of tandem differential mobility
18 analyser (TDMA) measurements, *Journal of Aerosol Science*, 40, 134-151, 2009.

19 Johnson, G. R., Ristovski, Z., and Morawska, L.: Method for measuring the
20 hygroscopic behaviour of lower volatility fractions in an internally mixed aerosol,
21 *Journal of Aerosol Science*, 35, 443-455, 2004.

22 Kaufman, Y., Hobbs, P., Kirchhoff, V., Artaxo, P., Remer, L., Holben, B., King, M.,
23 Ward, D., Prins, E., and Longo, K.: Smoke, Clouds, and Radiation - Brazil (SCAR -
24 B) experiment, *Journal of Geophysical Research: Atmospheres*, 103, 31783-31808,
25 1998.

26 Kondo, Y., Takegawa, N., Miyazaki, Y., Ko, M., Koike, M., Kita, K., Kawakami, S.,
27 Shirai, T., Ogawa, T., and Blake, D. R.: Effects of biomass burning and lightning on
28 atmospheric chemistry over Australia and South-east Asia, *International Journal of
29 Wildland Fire*, 12, 271-281, 2003.

30 Lawson, S. J., Keywood, M. D., Galbally, I. E., Gras, J. L., Caine, J. M., Cope, M. E.,
31 Krummel, P. B., Fraser, P. J., Steele, L. P., Bentley, S. T., Meyer, C. P., Ristovski, Z.,
32 and Goldstein, A. H.: Biomass burning emissions of trace gases and particles in marine
33 air at Cape Grim, Tasmania, *Atmospheric Chemistry and Physics*, 15, 13393-13411,
34 2015.

35 Levin, E., Prenni, A., Palm, B., Day, D., Campuzano-Jost, P., Winkler, P., Kreidenweis,
36 S., DeMott, P., Jimenez, J., and Smith, J.: Size-resolved aerosol composition and its
37 link to hygroscopicity at a forested site in Colorado, *Atmospheric Chemistry and
38 Physics*, 14, 2657-2667, 2014.

39 Mallet, M. D., Desservettaz, M. J., Miljevic, B., Milic, A., Ristovski, Z. D., Alroe, J.,
40 Cravigan, L. T., Jayaratne, E. R., Paton-Walsh, C., Griffith, D. W. T., Wilson, S. R.,
41 Kettlewell, G., van der Schoot, M. V., Selleck, P., Reisen, F., Lawson, S. J., Ward, J.,
42 Harnwell, J., Cheng, M., Gillett, R. W., Molloy, S. B., Howard, D., Nelson, P. F.,
43 Morrison, A. L., Edwards, G. C., Williams, A. G., Chambers, S. D., Werczynski, S.,
44 Williams, L. R., Winton, V. H. L., Atkinson, B., Wang, X., and Keywood, M. D.:
45 Biomass burning emissions in north Australia during the early dry season: an overview
46 of the 2014 SAFIRED campaign, *Atmospheric Chemistry and Physics Discussions*,
47 2016.

48 Milic, A., Mallet, M. D., Cravigan, L. T., Alroe, J., Ristovski, Z. D., Selleck, P.,
49 Lawson, S. J., Ward, J., Desservettaz, M. J., Paton-Walsh, C., Williams, L. R.,
50 Keywood, M. D., and Miljevic, B.: Aging of aerosols emitted from biomass burning in

1 northern Australia, *Atmospheric Chemistry and Physics Discussions*, 2016, 1-24,
2 10.5194/acp-2016-730, 2016.

3 Mircea, M., Facchini, M., Decesari, S., Cavalli, F., Emblico, L., Fuzzi, S., Vestin, A.,
4 Rissler, J., Swietlicki, E., and Frank, G.: Importance of the organic aerosol fraction for
5 modeling aerosol hygroscopic growth and activation: a case study in the Amazon Basin,
6 *Atmospheric Chemistry and Physics*, 5, 3111-3126, 2005.

7 Mochida, M., and Kawamura, K.: Hygroscopic properties of levoglucosan and related
8 organic compounds characteristic to biomass burning aerosol particles, *Journal of*
9 *Geophysical Research: Atmospheres* (1984–2012), 109, 2004.

10 Novakov, T., and Corrigan, C.: Cloud condensation nucleus activity of the organic
11 component of biomass smoke particles, *Geophysical Research Letters*, 23, 2141-2144,
12 1996.

13 Noziere, B.: Don't forget the surface, *Science*, 351, 1396-1397, 2016.

14 Paramonov, M., Aalto, P., Asmi, A., Prisle, N., Kerminen, V.-M., Kulmala, M., and
15 Petäjä, T.: The analysis of size-segregated cloud condensation nuclei counter (CCNC)
16 data and its implications for cloud droplet activation, *Atmospheric Chemistry and*
17 *Physics*, 13, 10285-10301, 2013.

18 Petters, M., and Kreidenweis, S.: A single parameter representation of hygroscopic
19 growth and cloud condensation nucleus activity, *Atmospheric Chemistry and Physics*,
20 7, 1961-1971, 2007.

21 Petters, M. D., Carrico, C. M., Kreidenweis, S. M., Prenni, A. J., DeMott, P. J., Collett,
22 J. L., and Moosmüller, H.: Cloud condensation nucleation activity of biomass burning
23 aerosol, *Journal of Geophysical Research: Atmospheres*, 114, 2009.

24 Platnick, S., and Twomey, S.: Determining the susceptibility of cloud albedo to changes
25 in droplet concentration with the Advanced Very High Resolution Radiometer, *Journal*
26 *of Applied Meteorology*, 33, 334-347, 1994.

27 Pöschl, U., Rose, D., and Andreae, M. O.: Climatologies of Cloud-related Aerosols.
28 Part 2: Particle Hygroscopicity and Cloud Condensation Nucleus Activity, in: *Clouds*
29 *in the Perturbed Climate System: Their Relationship to Energy Balance, Atmospheric*
30 *Dynamics, and Precipitation*, MIT Press, 58-72, 2009.

31 Pringle, K., Tost, H., Pozzer, A., Pöschl, U., and Lelieveld, J.: Global distribution of
32 the effective aerosol hygroscopicity parameter for CCN activation, *Atmospheric*
33 *Chemistry and Physics*, 10, 5241-5255, 2010.

34 Reid, J., Koppmann, R., Eck, T., and Eleuterio, D.: A review of biomass burning
35 emissions part II: intensive physical properties of biomass burning particles,
36 *Atmospheric Chemistry and Physics*, 5, 799-825, 2005.

37 Reutter, P., Su, H., Trentmann, J., Simmel, M., Rose, D., Gunthe, S., Wernli, H.,
38 Andreae, M., and Pöschl, U.: Aerosol-and updraft-limited regimes of cloud droplet
39 formation: influence of particle number, size and hygroscopicity on the activation of
40 cloud condensation nuclei (CCN), *Atmospheric Chemistry and Physics*, 9, 7067-7080,
41 2009.

42 Ristovski, Z. D., Wardoyo, A. Y., Morawska, L., Jamriska, M., Carr, S., and Johnson,
43 G.: Biomass burning influenced particle characteristics in Northern Territory Australia
44 based on airborne measurements, *Atmospheric Research*, 96, 103-109, 2010.

45 Rose, D., Nowak, A., Achtert, P., Wiedensohler, A., Hu, M., Shao, M., Zhang, Y.,
46 Andreae, M., and Pöschl, U.: Cloud condensation nuclei in polluted air and biomass
47 burning smoke near the mega-city Guangzhou, China—Part 1: Size-resolved
48 measurements and implications for the modeling of aerosol particle hygroscopicity and
49 CCN activity, *Atmospheric Chemistry and Physics*, 10, 3365-3383, 2010.

1 Rose, D., Gunthe, S. S., Su, H., Garland, R. M., Yang, H., Berghof, M., Cheng, Y. F.,
2 Wehner, B., Achtert, P., Nowak, A., Wiedensohler, A., Takegawa, N., Kondo, Y., Hu,
3 M., Zhang, Y., Andreae, M. O., and Poschl, U.: Cloud condensation nuclei in polluted
4 air and biomass burning smoke near the mega-city Guangzhou, China–Part 2: Size-
5 resolved aerosol chemical composition, diurnal cycles, and externally mixed weakly
6 CCN-active soot particles, *Atmospheric Chemistry and Physics*, 11, 2817-2836, 2011.
7 Russell-Smith, J., Yates, C. P., Whitehead, P. J., Smith, R., Craig, R., Allan, G. E.,
8 Thackway, R., Frakes, I., Cridland, S., and Meyer, M. C.: Bushfires ‘down under’:
9 patterns and implications of contemporary Australian landscape burning, *International*
10 *Journal of Wildland Fire*, 16, 361-377, 2007.
11 Spracklen, D., Carslaw, K., Pöschl, U., Rap, A., and Forster, P.: Global cloud
12 condensation nuclei influenced by carbonaceous combustion aerosol, *Atmospheric*
13 *Chemistry and Physics*, 11, 9067-9087, 2011.
14 Stokes, R., and Robinson, R.: Interactions in aqueous nonelectrolyte solutions. I.
15 Solute-solvent equilibria, *The Journal of Physical Chemistry*, 70, 2126-2131, 1966.
16 Twomey, S.: Aerosols, clouds and radiation, *Atmospheric Environment. Part A.*
17 *General Topics*, 25, 2435-2442, 1991.
18 van der Werf, G. R., Randerson, J. T., Giglio, L., Collatz, G. J., Kasibhatla, P. S., and
19 Arellano Jr, A. F.: Interannual variability in global biomass burning emissions from
20 1997 to 2004, *Atmospheric Chemistry and Physics*, 6, 3423-3441, 2006.
21 Ward, D., Kloster, S., Mahowald, N., Rogers, B., Randerson, J., and Hess, P.: The
22 changing radiative forcing of fires: global model estimates for past, present and future,
23 *Atmospheric Chemistry and Physics*, 12, 2012.
24 Warner, J., and Twomey, S.: The production of cloud nuclei by cane fires and the effect
25 on cloud droplet concentration, *Journal of the Atmospheric Sciences*, 24, 704-706,
26 1967.
27 Winton, V. H. L., Edwards, R., Bowie, A. R., Keywood, M., Williams, A. G.,
28 Chambers, S. D., Selleck, P. W., Desservettaz, M., Mallet, M. D., and Paton-Walsh, C.:
29 Dry season aerosol iron solubility in tropical northern Australia, *Atmospheric*
30 *Chemistry and Physics*, 16, 12829, 2016.
31
32